Vibrational Energy Harvester with Metglas for Air Vehicle Applications

Undergraduate Honors Thesis

Presented in Partial Fulfillment of the Requirements for Graduation with Distinction at
The Ohio State University

By
Sylvia G. Cressman

* * * * *

The Ohio State University
2022

Examination Committee:

Dr. Marcelo Dapino, Adviser

Dr. Hanna Cho

Approved By:

_____

Advisor Undergraduate Program
in Mechanical Engineering

Abstract

Lightweight air vehicles such as drones, kites, and weather balloons require active wind monitoring devices for flight control. However, current aircraft wind monitoring devices such as cup anemometers, pitot tubes, and radiosondes tend to be large and heavy. As a result, they induce aerodynamic drag and often require additional power draw, reducing the aircraft's efficiency. To address these problems, a lightweight, self-powered wind sensor was developed for aircraft applications. In the first phase of this project, capacitive sensors and a magnetometer were integrated in an airfoil for wind speed and direction measurements. In the second phase, a wind energy harvesting subsystem was developed using Metglas, which is a magnetostrictive material that produces a magnetic field change when stressed. This change in magnetic field can be converted into electrical energy based on Faraday's law that states a voltage is induced in a coil exposed to a changing magnetic field. Metglas is a desirable material for energy conversion due to its strength and long cycle life. To better understand this material, unannealed Metglas 2826MB and Metglas 2605SA1 were placed in a clamped, cantilever beam setup. The resonant frequencies of the beam were determined both analytically and experimentally to find optimal vibration for power output. Vibrations were induced in the beam with a shaker and the output voltage produced was observed through a copper coil wrapped around the beam. In this setup, a Metglas/steel unimorph beam was proven to have energy conversion capabilities. Results from this study will help better understand vibrational power potential of all forms of Metglas, specifically unannealed variations. Knowing more of its controlled vibrational behavior can help to predict its power generation from vibrations due to wind or other sources, allowing it to be used for a variety of low power applications.

Acknowledgements

None of this project would have been possible if it weren't for the help of some influential individuals. First, I would like to express my gratitude to Dr. Marcelo Dapino who served as my advisor on this research project. He gave me the chance and the freedom to pursue this project as an undergraduate along with many other projects along the way. I will be forever grateful for the opportunities I have received from him and the technical growth I have been able to achieve over my years of working in his lab. Next, I would like to thank all my colleagues in the Smart Materials and Structures Lab group both past and present. I am incredibly thankful for the help and patience you all have given me throughout my time in the lab. I would especially like to thank Dr. Leon Headings, Brad Losey, Dr. Arun Ramanathan, Ismail Nas, and Vivek Srinivas who taught me what it means to do research and how to enjoy doing it. I express my thanks to Dr. Hanna Cho for serving on my defense committee. I also would like to express thanks to the mechanical engineering department at Ohio State for providing me with many wonderful experiences over the past four years.

Outside of mechanical engineering, I am grateful for my friends and family who have brought joy to my whole college career and life. To my friends: Anna, Collin, Emily, Mitali, thanks for all the laughs, support, and great memories. College wouldn't have been the same without you. To my extended family: thanks for your constant encouragement from both near and far away. To my sisters: Sophie and Dana, thanks for motivating me to achieve big things and giving me someone to turn to every step of the way. To my parents: Heidi and Mark, thanks for your constant, unwavering support in everything I do, nothing in my life would have been possible without you.

Table of Contents

List of Tables

List of Figures

Chapter 1: Introduction

1.1 Background

As the mobility industry incorporates new types of lightweight vehicles, there is a growing interest in improving the efficiency of small drones, kites, and balloons. What always remains a necessity in these aircraft is active wind monitoring systems; so they may maintain stability in conditions ranging from light breezes to hurricanes. Aircraft such as airplanes, use pitot tubes for airspeed measurements, however, these devices are prone to icing. Because they operate at high altitudes, ice buildup progressively occurs and can render pitot tubes inoperable. Therefore, they require additional ice sensing devices that require additional power draw from the aircraft as well as more sophisticated deicing techniques [1]. Other aircraft such as weather balloons utilize radiosonde devices which communicate wind data via radar, GPS, or radio-direction finders. Wind monitoring is also achieved through anemometers both on land and in drones. These commercial anemometers come in the forms of cup, thermal, and ultrasonic devices. Cup anemometers are bulky, inducing additional drag especially in an aircraft [2] as well as have slow response time which is not optimal for in-flight instrumentation [3]. Other commercially available anemometers such as sonic anemometers are difficult to calibrate and accurately collect data from due to inconsistencies found in their measurements [4].

To address these issues with current wind monitoring systems and in an effort to continue to advance the efficiency of lightweight air vehicles, a new wind monitoring system needed to be investigated to ensure lightweight, low-drag, self-powered qualities. In the first phase of this research, a magnetometer paired with a capacitive pressure skin incorporated into an aerodynamic airfoil were utilized for achieving the wind sensing needs. In the second phase, which this thesis

project focused on, wind energy harvesting was studied to supply voltage to the sensor system and reduce its power draw. An overview of this project is shown in Figure 1.

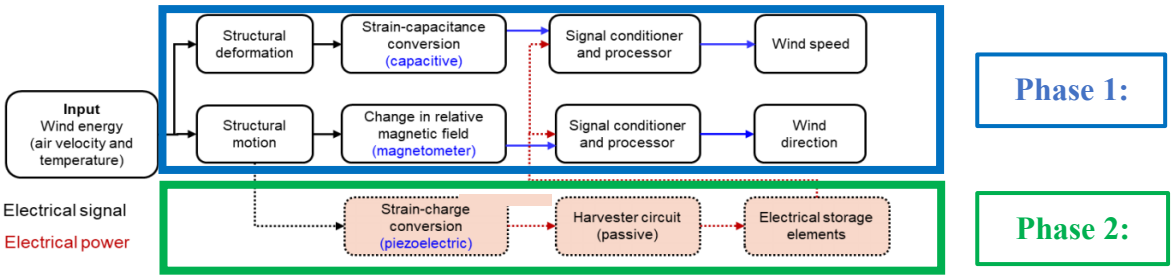

Figure 1: Wind sensor system project goal

Energy harvesting is the transformation of environmental energy such as mechanical, thermal, solar, wind, etc. to electrical energy using materials or mechanisms of conversion. Such materials and methods of transformation include photovoltaics to convert solar energy, thermoelectrics to convert thermal energy, and electromechanical transducers to convert mechanical or kinetic energy [5]. The typical parts of an energy harvesting sensor system can be seen in Figure 2.

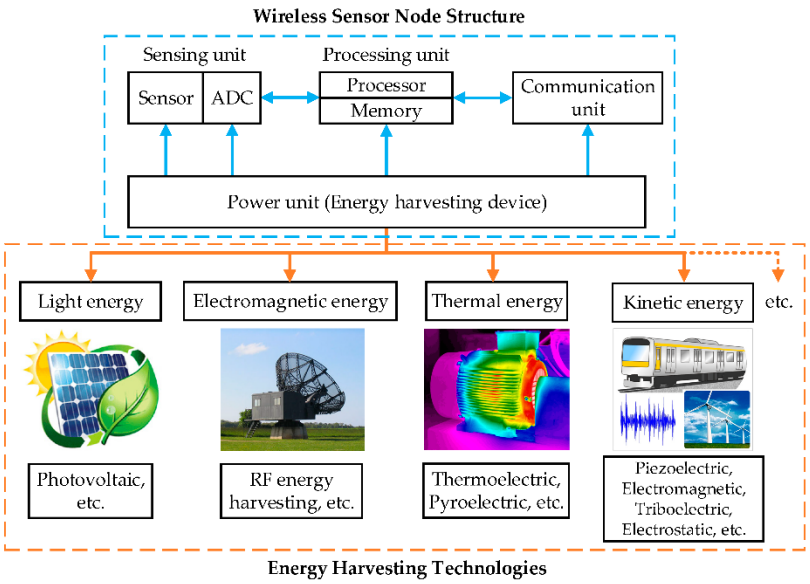

Figure 2: Energy harvesting system overview[6]

Electromechanical or kinetic transduction can help to harness structural vibrations that may otherwise be considered waste energy. This transduction can be achieved through a wide variety of materials and techniques. One technique, electromagnetic energy harvesting, employs a conductor moving through a magnetic field while wrapped in a coil to create an inductor. Another technique, electrostatic energy harvesting, utilizes vibrational movement to separate capacitor plates or change the area between them. This causes a change in capacitance that can increase a system's voltage.

Other techniques rely on the use of smart materials, including piezoelectric and magnetostrictive materials. Smart materials have changing material properties in response to physical (temperature, electric fields, magnetic fields, etc.), chemical, or biological stimuli. Once these stimuli are removed, the materials go back to their original state [7]. Piezoelectric materials generate an electrical charge when placed under mechanical stresses, with the reverse effect also being true. A voltage can directly be produced when piezoelectric materials are subjected to stresses. Magnetostrictive materials exhibit a magnetization change when they are subjected to

mechanical stress. Because magnetostrictive materials do not directly produce a voltage or current when stressed, they require additional methods to convert magnetic field change into voltage. One method is through Faraday's law, which states that an electromotive force is induced in a closed electrical conductor exposed to an alternating magnetic field. A magnetic field change can be caused for instance, by variable magnetic field source or a rotating a coil relative to a magnet. Such wireless power transmission can be advantageous in a variety of situations including energy harvesting and actuation.

1.2 Literature Review

1.2.1 Magnetostrictive Fundamentals

Magnetostriction was discovered by James Joule in 1842 from his observation of iron bar elongation in the presence of magnetic fields. Magnetostriction is defined as the strain exhibited by a magnetic material when it is exposed to a magnetic field [8]. Emilio Villari in 1864 discovered the reverse effect whereby a stress induces a magnetic field change [9]. This effect, called the Villari effect, is the basis for magnetostrictive energy harvesting techniques. Common magnetostrictive materials include iron, cobalt, and nickel although many ferromagnetic materials display some degree of magnetostriction. The small energy conversion of these other materials makes them impractical for sensing, actuating, and energy harvesting methods.

Magnetostrictive materials are assumed to have a structure of non-interacting magnetic domains under the Stoner-Wohlfarth approximation. Under this approximation, each domain has a separate magnetization that combines together in a weighted sum to form the bulk magnetization of a material. Under mechanical compression, domains are forced to align perpendicular to the force, which gives the material zero bulk magnetization [10]. Once the compression is released,

the material goes back to its demagnetized state. Mechanical stress loading can be achieved through various means including clamped cantilevered beams under vibration. In this scenario, parts of the beam cyclically undergo compression and tension with the bulk magnetization also cyclically changing. Mechanical stresses affect the magnetization of a magnetostrictive material, but magnetic fields also play a role. Under a magnetic field, the magnetic domains align parallel to the field direction. Such alignment creates maximum bulk magnetization parallel to the magnetic field. Combined balancing of mechanical stress and magnetic field can achieve maximum bulk magnetization changes in magnetostrictive materials. These two parts working in conjunction are shown in Figure 3, where H_0 is an applied or bias magnetic field. For magnetostrictive materials, high magnetization change is achieved relative to other materials due to 90 degree domain rotation [10]. To achieve enhanced domain alignment in vibrational situations, a bias magnetic field is often applied to magnetostrictive materials. The bias magnetic field commonly is applied through permanent magnets.

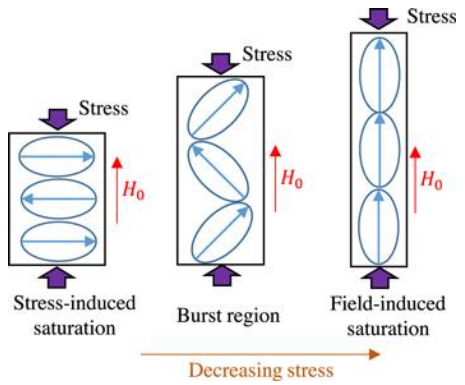

Figure 3: Stress and applied magnetic field effect on magnetostrictive material domains [10]

1.2.2 Magnetostrictive Energy Conversion

To transform the change in magnetic field from a magnetostrictive material undergoing mechanical stresses into a voltage, a pickup coil is employed surrounding the material. Faraday's

law becomes in effect allowing a change in the magnetic environment of the coil to induce a voltage in the coil. The induced voltage is outlined in equations (1) and (2), where V is the induced voltage, Φ is the magnetic flux through the coil, N is the number of turns in the coil, A is the coil's cross section, and B is the magnetic flux density.

$$V = -N\left(\frac{d\Phi}{dt}\right) \tag{1}$$

$$\mathrm{V} = -\mathrm{NA}\left(\frac{dB}{dt}\right) \tag{2}$$

The voltage output of the coil can then be connected to a harvesting circuit for sensor or conditioning usage. In magnetostrictive harvesting investigations, to assess power output, often times the coil drives a resistive load. The whole energy harvesting system can be thought of in terms of electrical components as shown in Figure 4, where R_c is the pickup coil resistance, L_c is the pickup coil inductance, R_l is the resistance of the load, and V_{open} is the open circuit voltage being measured. It has previously been shown that for magnetostrictive materials such as Metglas and Galfenol the load impedance affects the power output of the system, so it must be selected accordingly [11,12].

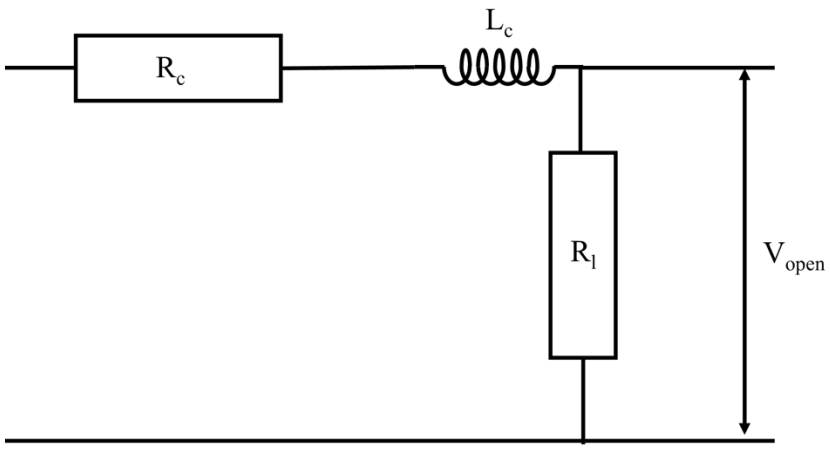

Figure 4: Equivalent electrical circuit of energy harvesting system

The power output in many magnetostrictive harvesting experiments is converted to power density. This measure normalizes the power output making it easier for comparison among materials. It is common to find in the literature power density using just the active layers of the magnetostrictive material. Power density can be calculated from maximum power or average power as shown in equations (3) and (4),where PD_{peak} is peak power density, P_{max} is the maximum power output of the system, and V_{act} is the volume of the active material. PD_{avg} is the average power density where P_{avg} is the average output power.

$$PD_{peak} = \left(\frac{P_{max}}{V_{act}}\right) \tag{3}$$

$$PD_{avg} = \left(\frac{P_{avg}}{V_{act}}\right) \tag{4}$$

P_{avg} is calculated using equations (5) and (6), where W_{out} is the electrical power consumed

by the circuit, R_L is the harvesting circuit's resistance across which voltage V_0 is measured, and T_0 is the period of the input stress.

$$P_{avg} = \left(\frac{W_{out}}{T_0}\right) \tag{5}$$

$$W_{out} = \int_0^{T_0} \frac{V_0(t)^2}{R_L} dt \tag{6}$$

1.2.3 Magnetostrictive Metglas Material Overview

Piezoelectric materials currently dominate in the field of energy harvesting due to their availability and easy compatibility with electromechanical systems without the need for additional transduction beyond the material. However, piezoelectric materials suffer from various drawbacks. Piezoelectrics are brittle ceramics prone to aging degradation. Additionally, they exhibit depolarization above their Curie temperature [13]. On the contrary, Metglas is a magnetostrictive material that exhibits high flexibility, no depolarization [11], high energy conversion efficiency, and long life[14]. These characteristics make it a promising material for energy harvesting techniques.

Metglas is a thin ribbon iron-based metal alloy produced by rapid solidification of the molten alloy. This rapid cooling process makes it an amorphous metal, which means that unlike other metals, all of its atoms are randomly arranged without forming a crystalline structure. This puts it into a metastable condition which allows it to have higher permeability and low losses [15]. It is known as metallic glass for this disordered atomic structure similar to other metallic oxide based glasses. Metglas is primarily iron based coming in a range alloy compositions such as Metglas 2605SA1 (Fe_{80} Si_9 B_{11}), Metglas 2705M ($Co_{69}Fe_4Ni_1Mo_2B_{12}Si_{12}$), and Metglas 2826MB

($Fe_{40}Ni_{38}Mo_4B_1$). As shown in Table 1, Metglas exhibits modulus of elasticities between 100-110 GPa which is a similar stiffness to other magnetostrictive materials. It also has an extremely high permeability which can be useful to amplify magnetic changes, high magnetic coupling coefficient, and a high tensile strength. These characteristics make it a better suited magnetostrictive material for certain applications such as the proposed wind sensing system.

Table 1: Magnetostrictive Material Property Comparison

Material Property	**Metglas 2826 MB**	**Metglas 2605SA1**	**Terfenol-D ($Tb_{.3}Dy_{.7}Fe_2$)**	**Galfenol ($Fe_{81.6}Ga_{18.4}$)**	**Steel**
Modulus of Elasticity (GPa)	100-110[16]	100-110[16]	43[17]	40-60[18]	200 [19]
Tensile Strength (GPa)	1-2[16]	1-2[16]	0.028[20]	0.35[18]	0.4-0.550[21]
Relative Magnetic Permeability	50,000[16]	45,000[16]	2-10[22]	75-100[18]	100[23]
Coupling Coefficient	0.98[24]	0.98[24]	0.7-0.8[20]	0.6-0.7[18]	-
Magnetostriction Constant (ppm)	12[16]	27[16]	800-1200 [20]	200-250[18]	-
Density (g/cm^3)	7.90[16]	7.18[16]	9.25[20]	7.80[18]	7.87[19]
Thermal Expansion (ppm/ºC)	11.7[16]	7.6[16]	11[22]	11[18]	9E-6[25]
Curie Temperature (ºC)	353[16]	395[16]	380[22]	670[18]	770[26]

1.2.4 Previous Metglas Experiments

Metglas' suitability for energy harvesting has been explored analytically, computationally, and experimentally. Jafari *et al.* utilized Metglas 2605SC ($Fe_{81}B_{13.5}Si_{3.5}C_2$) layered on stainless steel to develop a model validated through experimentation of voltage output. This proved Metglas' potential use in low frequency ranges [27]. Such a low frequency operating range is suitable for wind energy harvesting from a cantilever. Other experiments have looked at the effect of beam parameters on Metglas. Mohammadi and Esfandiari [14] used numerical predictions on Metglas 2605SC ribbons paired with various substrate materials and harvesting circuit resistances to determine an optimal harvesting setup without a magnetic bias. They utilized a high harvesting resistance with steel to obtain a maximum power output [14]. Through experimentation, some studies have looked at ways to reduce the need for a bias magnetic field. Wang and Yuan annealed Metglas 2605SC under a magnetic field to mitigate the need for a magnetic bias and experimentally achieved a power density of 900 μWcm^{-3} with a printed circuit board harvester [11]. Other studies have focused on Metglas in practical applications such as Tan *et al.* who scavenged from this material in a bone compressive setup [28]. However, there is still a need to better understand various unannealed Metglas materials' vibrational energy harvesting behavior and directly compare different Metglas forms in a controlled vibrational setting which can later help with noncontrolled environment predictions. Being able to directly compare materials and parameters can help to make informed decisions on material choice for not only the wind sensor system but other sensor power applications.

1.3 Project Objectives

In this research project, the initial developmental steps to create a self-powered wind sensor system for air vehicle applications using wind energy harvesting techniques were achieved. The first objective was to vibrationally characterize different Metglas materials and harvesting configurations in a controlled environment. Beams with single and multiple Metglas 2826MB and 2605SA1 layers were experimentally looked at to understand and validate their vibrational behavior in comparison to fundamental beam bending equations. As part of this, an experimental setup was developed and calibrated. Displacement sensing and voltage transduction to a coil were explored as vibrational characterization techniques. In an effort to optimize power output potential in a variety of vibrational situations, Metglas materials including 2826Mb and 2605SA1 were directly compared along with parameters such as bias magnetic field presence. This allowed for comparison of the materials to each other for power capabilities.

Chapter 2: Metglas Vibrational Characterization

All structures have an inherent set of natural frequencies or frequencies at which the system tends to oscillate. When a structure is excited at a frequency close to its natural frequency, assuming small damping of the system, a phenomenon called resonance is observed. At resonance, the structure's oscillations are amplified, making this an optimal frequency for energy harvesting. For this research, a clamped-free cantilever beam structure was selected due to its design simplicity for sensor system implementation and previous proven experimental energy harvesting capabilities for a variety of materials including Metglas. There exist equations to determine a beam's natural frequencies. However, it is also important that experimental tests be run on a beam since it will not exhibit perfect clamping or bending qualities due to inherent material and setup inaccuracies. The details of a Metglas and stainless steel unimorph beam calculations and experimental analysis are outlined below.

2.1 Cantilever Beam Description

In this research, Metglas 2826MB ($Fe_{40}Ni_{38}Mo_4B_1$) and Metglas 2605SA1 (Fe_{80} Si_9 B_{11}) ribbons were layered on separate stainless steel grade 316 beams. This Metglas was from Metglas®, Inc (https://metglas.com/magnetic-materials/). Initially, one Metglas 2826MB layer was adhered to the 0.02 inch thick stainless steel beam using epoxy (JB-WELD Clearweld). A unimorph beam design with stainless steel as a substrate was selected due to Metglas' ductility. With preliminary testing, just layered Metglas proved to flex greatly in a resting position under its

own weight, which is not desirable for beam deflection measurements. Thus, stainless steel 316 was selected as a substrate because it is not only stiffer, but also a non-magnetic material, ensuring that its presence would not interfere with Metglas' magnetic field. In addition, stainless steel has previously been shown to be one of the best substrates for Metglas energy harvesting with Metglas 2605SC [14]. The single layer Metglas unimorph beam is pictured in Figure 5. Later, four layers of Metglas were laminated on the stainless steel substrate to improve energy harvesting capabilities as previous magnetostrictive experiments such as those on Galfenol showed improved power generation with increased thickness ratio to a limit [29]. An aluminum tip mass was added to the beam to reduce the beams' first natural frequencies. An example image of this beam is in Figure 6. The actual dimensions of all of the Metglas cantilever beams created are shown in Table 2 where the effective length of each beam is the length of the beam that was not within the clamp during experimentation.

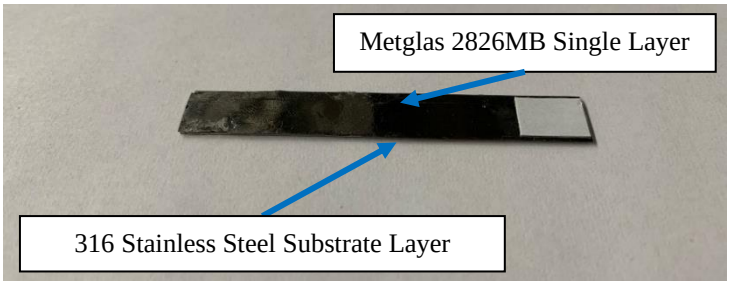

Figure 5: Metglas one layer unimorph beam

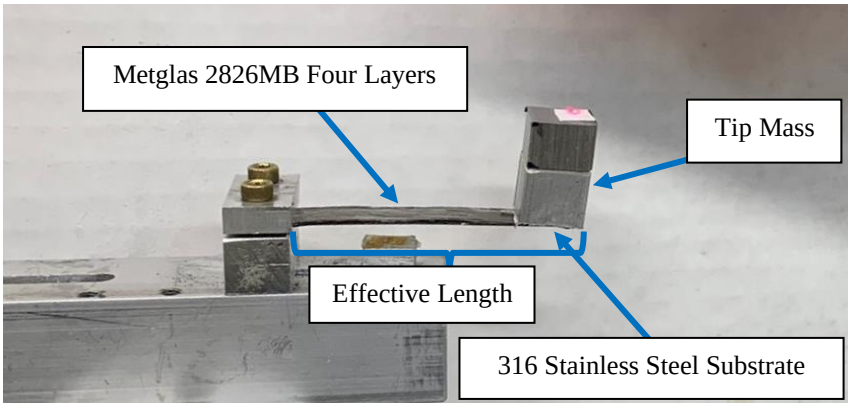

Figure 6: Metglas four layered unimorph beam with tip mass

Table 2: Cantilever beam dimensions

Beam	Unimorph Beam Length: mm (in)	Unimorph Beam Effective Length: mm (in)	Unimorph Beam Width: mm (in)	Unimorph Beam Stainless Steel Layer Thickness: mm (in)	Unimorph Beam Total Thickness: mm (in)	Tip Mass Weight: g (lb)
One Layer: Metglas 2826MB	65.786 (2.590)	53.975 (2.125)	9.449 (0.372)	0.508 (0.020)	0.510 (0.020)	-
Four Layers: Metglas 2826MB with tip mass	64.846 (2.553)	52.375 (2.062)	10.084 (0.397)	0.508 (0.020)	0.838 (0.033)	11.280 (0.0249)
Four Layers: Metglas 2605SA1 with tip mass	65.786 (2.590)	52.197 (2.055)	10.439 (0.411)	.508 (0.020)	1.016 (0.040)	10.960 (0.0242)

2.2 Cantilever Beam Theoretical Calculations

To obtain an initial idea of the potential natural frequency range of a Metglas and stainless steel unimorph beam, calculations of first natural frequency were performed. The Bernoulli-Euler-Timoshenko beam theories were utilized which assume no shear deformation or rotational inertia in the beam. In addition to these assumptions, further assumptions were made to simplify equations. As shown in Table 3, 316 stainless steel is about 17.5 times thicker than Metglas 2826MB and 22 times thicker than Metglas 2605SA1. As a result of this size difference, the beam calculations assume only a stainless steel 316 beam bending, without the additional qualities of

the Metglas laminates. Thus, the thickness of the beam utilized for calculations was just the thickness of the steel, or 0.02 inches.

Table 3: Beam material thicknesses

Material	**Thickness (μm)**
Metglas 2826MB Ribbon	29 [16]
Metglas 2605SA1 Ribbon	23[16]
Stainless Steel 316 Sheet	508

Calculations were first performed for a beam without a tip mass. This was done using equation (7) and equation (8) that calculate for a clamped-free cantilever beam.

$$f_1 = \frac{(1.87510407)^2}{2\pi L^2}\sqrt{\frac{EI}{m}} \tag{7}$$

$$I = \frac{bd^3}{12} \tag{8}$$

Here, L is the length of the beam, E is the modulus of elasticity, I is the area moment of inertia, m is the mass per unit length of the beam, b is the beam width, and d is the beam thickness. Let it be noted that the length of the beam utilized was the effective length of the beam or the part of the beam assumed to not be within the clamp. The parameter values input in these equations are shown in Table 4. Using stainless steel for the material properties and the dimensions shown previously in Table 2, for the 2826MB unimorph beam without a tip mass, the predicted first natural frequency was 140.221 Hz.

Table 4: Beam calculation constant input parameters

Parameter	Value	Unit
E, modulus of elasticity	197.5	GPa
ρ, density of beam material	7.97	g/cm^3
d, beam thickness	0.020	in

In an effort to reduce this first natural frequency to understand Metglas behavior in lower frequency situations, a tip mass was added to cantilevered beams of both types of Metglas. As a result, the beams became beams with concentrated masses as outlined in Figure 7, where M_b is the mass of the beam and M_t is the mass added to the tip. The first natural frequency equation of such a beam then becomes approximately equation (9) solved for by Blevins using a Rayleigh technique [19]. With all of the parameters the same as in equations (7) and (8), with tip masses, the expected first natural frequency values are 31.238 Hz and 32.366 Hz respectively.

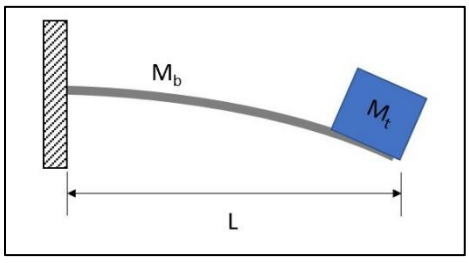

Figure 7: Cantilever beam with tip mass

$$f_1 = \frac{1}{2\pi}\sqrt{\frac{3EI}{L^3(M_p + .24M_b)}} \tag{9}$$

2.3 Experimental Setup Vibrational Characterization

The measurement system for the vibrational characterization utilized a flow of data outlined in Figure 8. The beam was held in a clamped cantilevered beam setup with a piece of white tape added to its end for ease of measurement through the laser displacement sensor. The unimorph beam was instantaneously excited using a quick imparted impulse. A Keyence LK G32 laser displacement sensor measured the beam's movement by returning a voltage value in the range of -10 to 10 V representing a -5 to 5 mm range of motion. This sensor was held in place using a 3D modelled and printed sensor holder in a metal apparatus which was bolted to the table to ensure stability as pictured in the experiment setup in Figure 9: Vibrational characterization setup . The laser sensor voltage output was collected through a National Instruments Corporation myDAQ system and LabVIEW 2021 software at an 11kHz sampling rate. Within LabVIEW, spectral data was collected using a peak measurement and Hanning window. This was collected for peak frequency cross comparison with results obtained through Matlab. On Matlab, the laser sensor voltage over time was analyzed using a fast Fourier transform (fft) built in function. The results of the fast Fourier transform were used to create a frequency spectrum plot that showed peaks at the beam's natural frequency. The first peak could then presumably be compared to the previously calculated theoretical values.

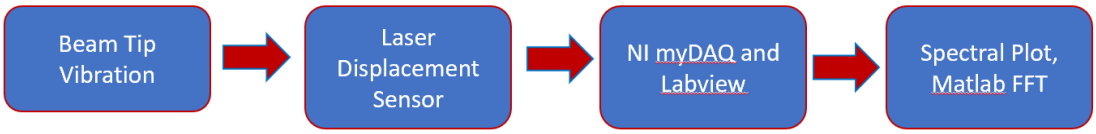

Figure 8: Overview of measurement schema for vibrational characterization

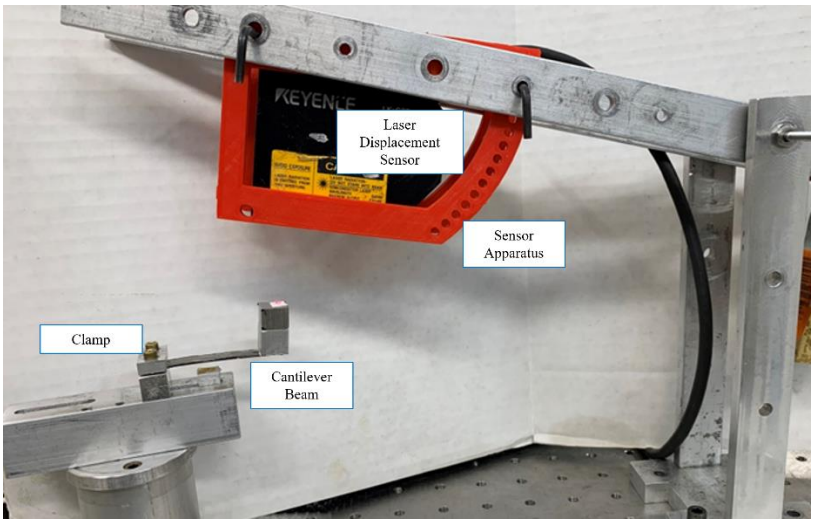

Figure 9: Vibrational characterization setup

Before testing initiated, calibration of the Keyence LK G32 sensor was performed. This was done through exciting the beam at a known frequency and reviewing the sensor output to ensure the peaks of displacement formed a matching frequency. The beam was excited using an electromagnetic shaker which was further used and will be outlined in the energy harvesting test setup section.

2.4 Metglas Vibrational Characterization Results and Discussion

Multiple trials were run on each beam using the test setup and procedure previously described to ensure accuracy of results. For the one layer Metglas 2826MB unimorph beam, the beam displacement over time is shown in Figure 10. The overall oscillation of the beam as it freely vibrated ending in a resting state proves the efficacy of the laser displacement sensor for these experiments. There are some occasional spikes in the displacement of the beam, which could potentially be due to the overall sensitivity of the laser system. The Keyence G32 laser sensor has a resolution of 2 mV according to manufacturer specifications. While the peak-to-peak data points measured were above this range, they are still within a 10 mV range, which nears this resolution.

Additionally, the sensor was run through a Keyence display unit before being input into the DAQ system. This added extra non shielded wiring that may have also incurred noise from the environment. Overall, the data follows a trend to what would be expected in a damped second order system as the displacement decays over time, so the spikes of data are considered non influential.

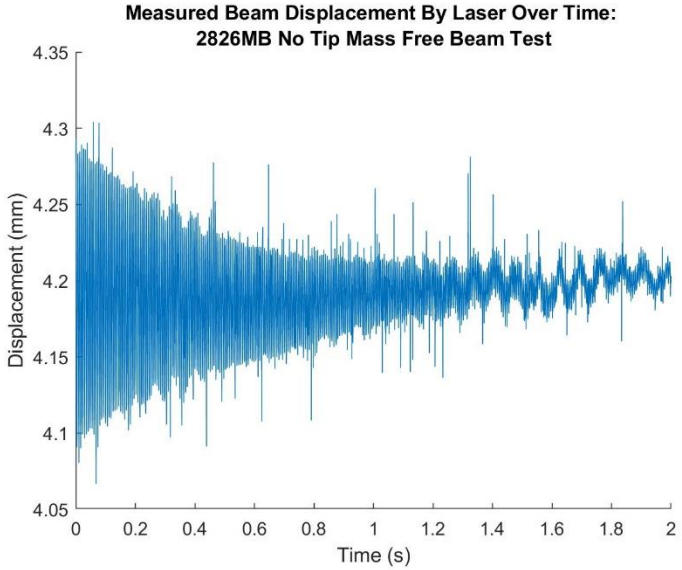

Figure 10: Metglas 2826MB no tip mass free beam test displacement

With a damped second order system, the damping can be numerically analyzed by determining the damping ratio of the system. The damping ratio is expected to be between a value of 0 and 1 for this beam deflection since it is an underdamped system. To find the damping ratio, a logarithmic decrement technique was used which is outlined in equations (9) and (10) with the data normalized around 0. In these equations, δ is the logarithmic decrement, x_n is a peak observed in the data, x_{n+1} is the proceeding peak observed, and ζ is the damping ratio or damping factor. For the one layer Metglas 2826MB beam, the damping ratio was found to be low at 0.0077, which is represented in the plot as the beam's movement slowly decayed.

$$\delta = ln\frac{x_n}{x_{n+1}} \tag{9}$$

$$\zeta = \frac{\delta}{\sqrt{4\pi^2 + \delta^2}} \tag{10}$$

The laser displacement output data was then assessed in Matlab to generate an amplitude spectrum. This spectrum is shown in Figure 11 with a noticeable first peak shown at 156.364 Hz. This peak is comparable to the theoretical first natural frequency of 140.221 Hz calculated in section 2.2 using the beam dimensions. As a verification, in LabVIEW, spectral data using peak magnitude settings was generated which is outlined in Figure 12. A peak is observed at a frequency of 156.016 Hz which confirms and validates the fast Fourier method utilized in the Matlab analysis.

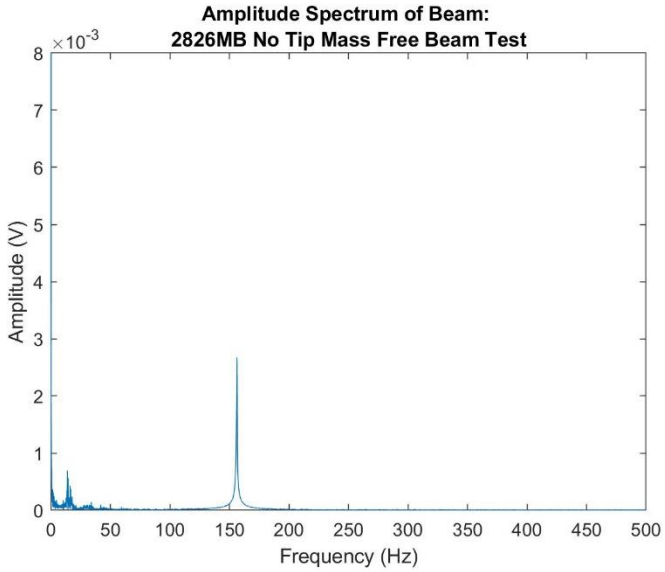

Figure 11: Matlab generated amplitude spectrum of 2826MB beam with no mass

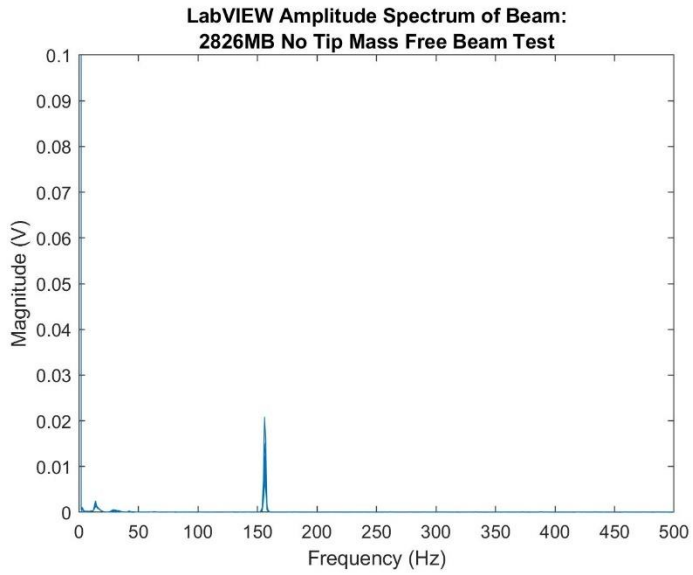

Figure 12: LabVIEW generated magnitude spectrum of 2826MB beam with no mass

When the tip mass was added along with the additional three Metglas 2826MB layers, the noise spikes from the laser sensor improved, resulting in a smoother displacement signal expressed in Figure 13. This is perhaps due to the beam having lowered natural frequencies and more damped motion. The beam's displacement goes up slightly before flattening which may be due to the beam's resting position not being exactly at 180 degrees. Using the previously outlined logarithmic decrement model, this damped system had a damping ratio of 0.0340 which is slightly higher than the damping ratio with just one layer. This is illustrated in this beam's displacement as it rapidly goes from oscillating to a resting state when compared to the other beams. In Figure 14, the frequency spectrums generated through Matlab and LabVIEW are shown. For Metglas 2826MB, the first natural frequency was observed at 47.5000 Hz for both spectrum generations. This is slightly higher than the expected frequency of 31.238 Hz, possibly due to the Metglas layers and epoxy adding stiffness to the beam which were not accounted for in the equations, thus increasing its natural frequencies. For the layered Metglas 2605SA1 beam, similar results were obtained. The displacement of the beam reported fewer spikes in Figure 15, corroborating with the Metglas

2826MB beam and advocating for the use of the layered tip mass beam for the energy harvesting investigations. Both the LabVIEW and Matlab results conferred around a first natural frequency of about 51 Hz, which is larger than the predicted 32.366 Hz for this beam. However, it does maintain a similar trend to the theoretical predictions in that, based on the beam dimensions, the 2605SA1 should have a higher frequency than the 2826MB beam. Additionally, the 2605SA1 beam was found to have a slightly lower damping ratio of only 0.0125 as compared to the 2826MB beam with 0.0340. A comparison of the damping ratios of all beams is shown in Table 5.

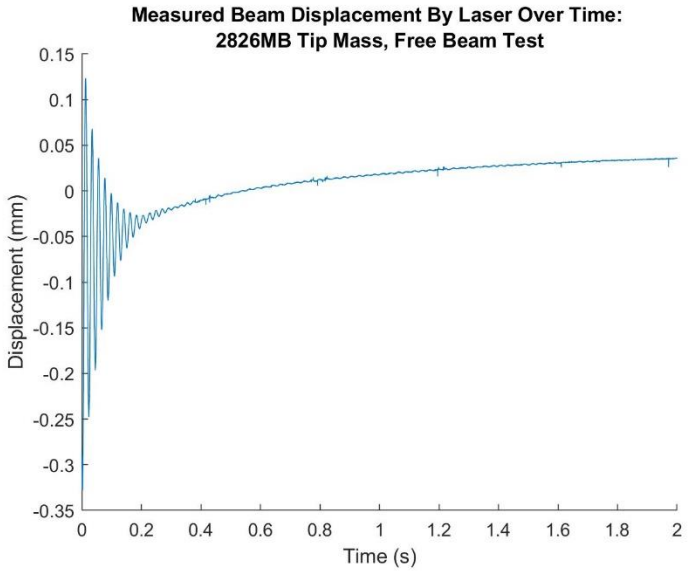

Figure 13: Layered 2826MB Metglas beam with tip mass displacement in free vibration

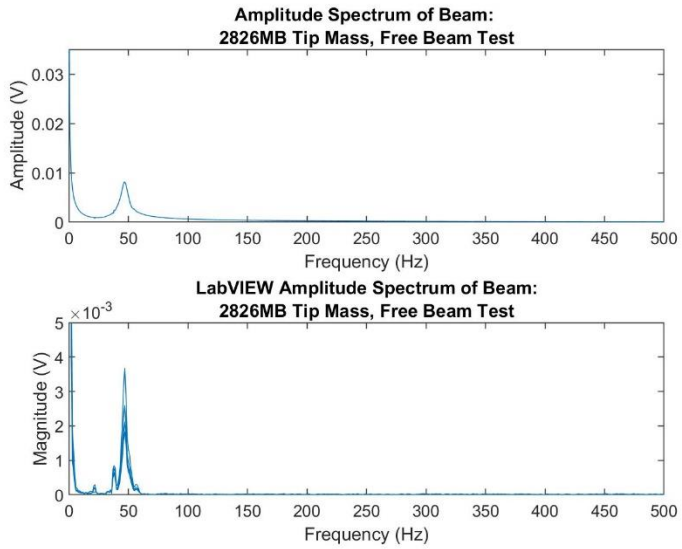

Figure 14: Layered 2826MB Metglas beam with tip mass frequency spectrums

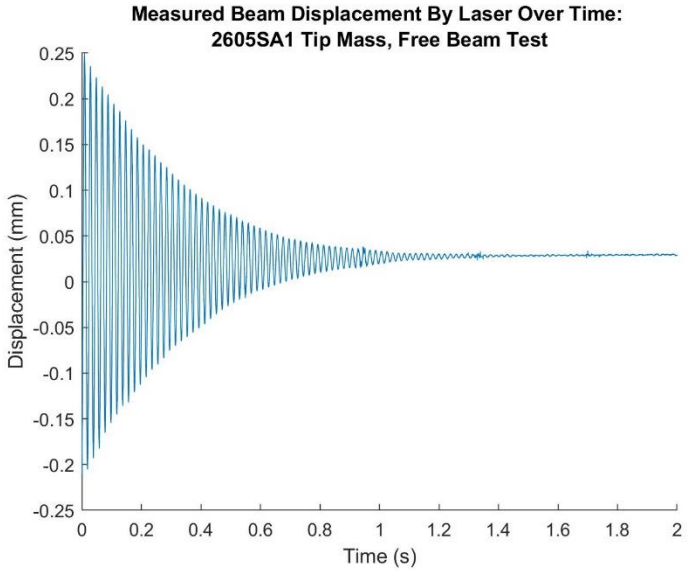

Figure 15: Layered 2605SA1 Metglas beam with tip mass displacement in free vibration

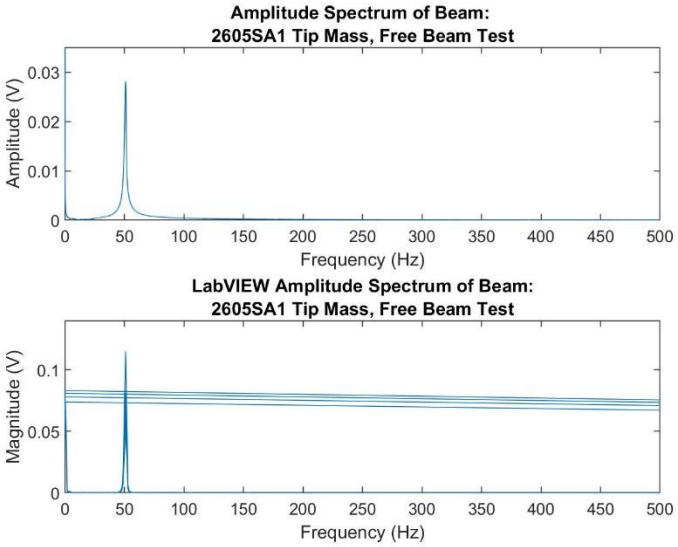

Figure 16: Layered 2605SA1 Metglas beam with tip mass frequency spectrums

Table 5: Damping ratio of beams

	Damping Ratio
1 Layer Metglas 2826MB	0.0077
4 Layer Metglas 2826MB with tip mass	0.034
4 Layer Metglas 2605SA1 with tip mass	0.0125

Table 6 provides an overview of the comparison between the expected theoretical first natural frequencies of the beams and the experimentally found first natural frequencies. The higher first natural frequency observed in experimental data may be due to the additional stiffness of the epoxy used to adhere the Metglas layers together. As noted in the beam calculations, many assumptions were utilized to simplify the model. Since there is a large

difference between the experimental and theoretical values, in the future more complex modelling could be explored to more accurately take into account the material qualities such as modulus of elasticity affected by the magnetostrictive layers as well as the epoxy. The Matlab fast Fourier transform method and LabVIEW autogenerating spectrum converge on similar values for the first natural frequencies of the beams, indicating that these spectral methods provide accurate results.

Table 6: Overview of theoretical and experimental Metglas beam first natural frequency values

Beam	**Theoretical First Natural Frequency (Hz)**	**Experimental First Natural Frequency Using Matlab FFT (Hz)**	**Experimental First Natural Frequency Using LabVIEW Spectrum (Hz)**
One Layer: Metglas 2826MB	140.221	156.3640	156.0160
Four Layers: Metglas 2826MB with tip mass	31.238	47.5000	47.0047
Four Layers: Metglas 2605SA1 with tip mass	32.366	51.0000	51.0051

Chapter 3: Metglas Energy Harvesting Capabilities

Different magnetostrictive materials, due to their properties, have varying capabilities of providing a changing magnetic environment needed for an induced voltage in a coil. In order to compare power generation capabilities of both Metglas 2826MB and 2605SA1, the same experiments and data were collected on both. First, the resonant frequencies observed in Chapter 2 were validated using a frequency sweep and maximum coil voltage. Then, beams were vibrated at their resonant frequencies to observe maximum power output. Power generation with the presence of a bias magnetic field was also explored and compared to the normal state of these unannealed materials. Knowing all of this data can help to prove or disprove scenarios in which these materials might be effective for energy harvesting or other applications.

3.1 Energy Harvesting Test Setup and Procedure

With Faraday's law in use to transduce between magnetic and electrical energy, the test setup focused on three main systems: electrical, mechanical, and magnetic. All of these systems worked in tandem to achieve the experimental setup necessary to measure the maximum voltage able to be harvested from unannealed Metglas 2826MB and unannealed Metglas 2605SA1. All of the systems used are pictured in Figure 17 and the flow of the experiment data is schematically outlined in Figure 18. An Agilent 33120A waveform generator was used to generate a sinusoidal wave, which was then amplified through an AE Techron 5050 Linear Amplifier. This amplified signal was input to an electromagnetic shaker and monitored with an oscilloscope. The shaker was placed on a rubber pad to help dampen its vibrations so as to not affect the displacement sensor readings. On top of the shaker was an aluminum stand on which the Metglas beam was clamped

with a coil around it. This aluminum stand kept the beam and coil free from the electromagnetic interference potential of the shaker.

The shaker provided a controlled vibrational environment for the clamped, cantilevered Metglas beam. The excitation and movement of the centrally placed beam induced a voltage in a pickup coil. The coil was fixed at a length of 1.235 inches with an inner diameter of 0.700 inches. It had 500 turns made from 32 American Wire Gauge wire. The coil output fed into a 220 Ohm harvesting circuit. This resistance was selected as previous Metglas experimentation observed an optimal resistance around 220 Ohms for annealed Metglas 3605SC for voltage output [11] and around 160 Ohms for a Metglas 3605SC and steel unimorph beam for optimal power output [14]. Voltages from the coil were read using a National Instruments myDAQ system into LabVIEW 2021 software at an 11 kHz sampling rate. Additionally, a Keyence LK G32 Displacement sensor was read into the DAQ system in an effort to continue to monitor the beam deflection. Its range was calibrated from -2 to 2 volts to represent -5 to 5 mm displacement.

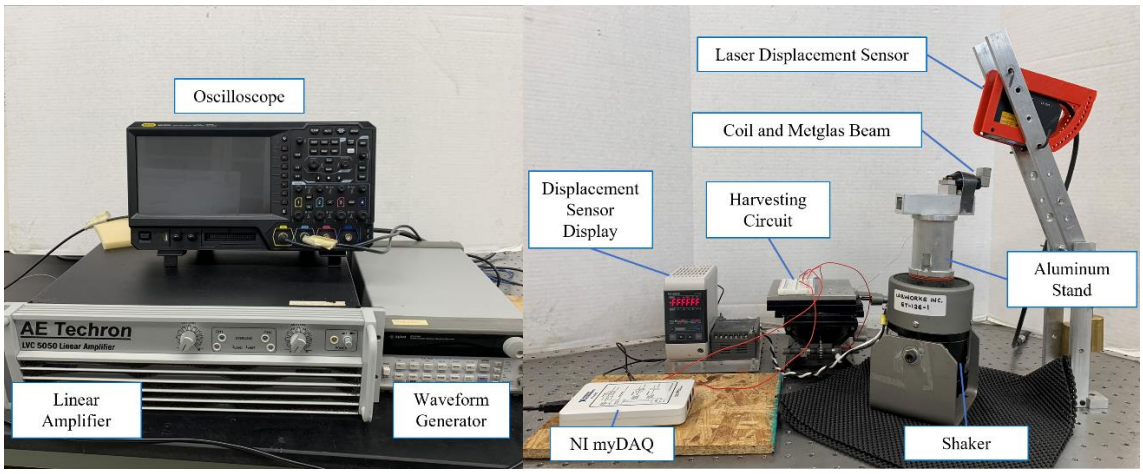

Figure 17: Test setup image

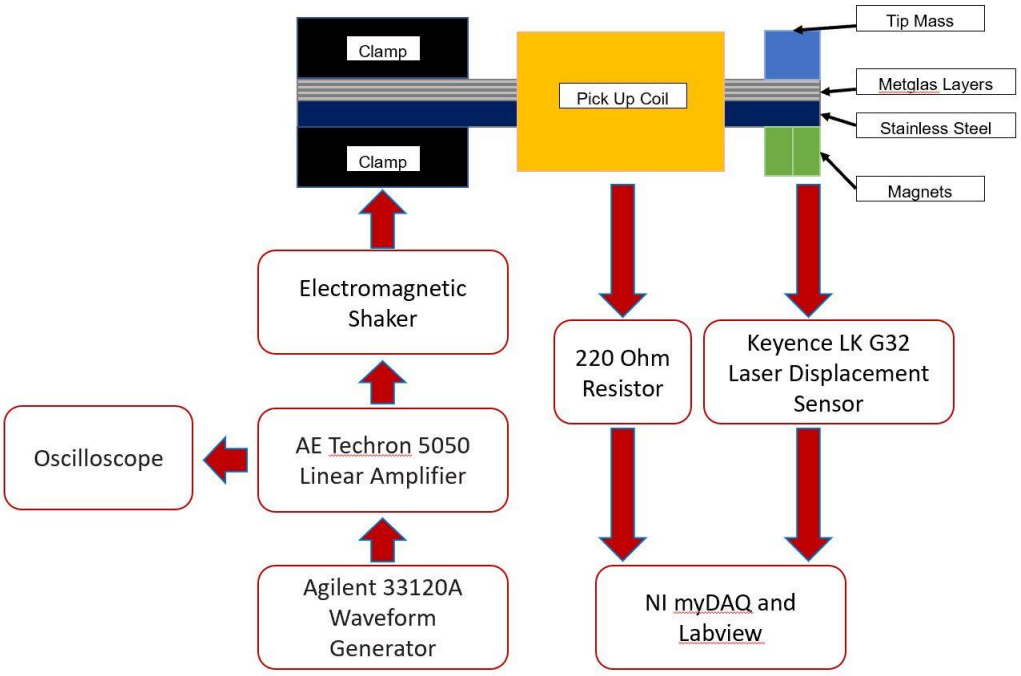

Figure 18: Overview of experimental flow

The four layered Metglas stainless steel uniform beams previously outlined in Table 2, were utilized in this experimentation. First, these beams were vibrated through a range of frequencies 1-800 Hz. The frequency of maximum coil voltage was determined to be the first resonant frequency of the beam. This value was compared to the previously calculated and the experimental found value from Chapter 2, to ensure continued accuracy. To find maximum voltage output and power output, the beam was then vibrated, through the shaker, at its observed first resonant frequency found through the coil. The maximum voltage harvested from the beam was determined to be the maximum voltage and power output of this material.

Additionally, to investigate the effect of a bias magnetic field on both Metglas 2826MB and Metglas 2605SA1, magnets were added to the beam tip. Two commercially available ceramic magnets generating 0.136 T of size 7/8 inch x 3/8 inch x 1/4 inch [22.225 mm x 9.525 mm x 6.350

mm] were used to generate the bias field. These magnets added an additional 6.48 g to the beam system. As a result, with the tip magnets another frequency sweep from 1-800 Hz was conducted to determine the new resonance of the system. The same steps were then followed to determine maximum power output with the bias magnetic field enacting on the beam.

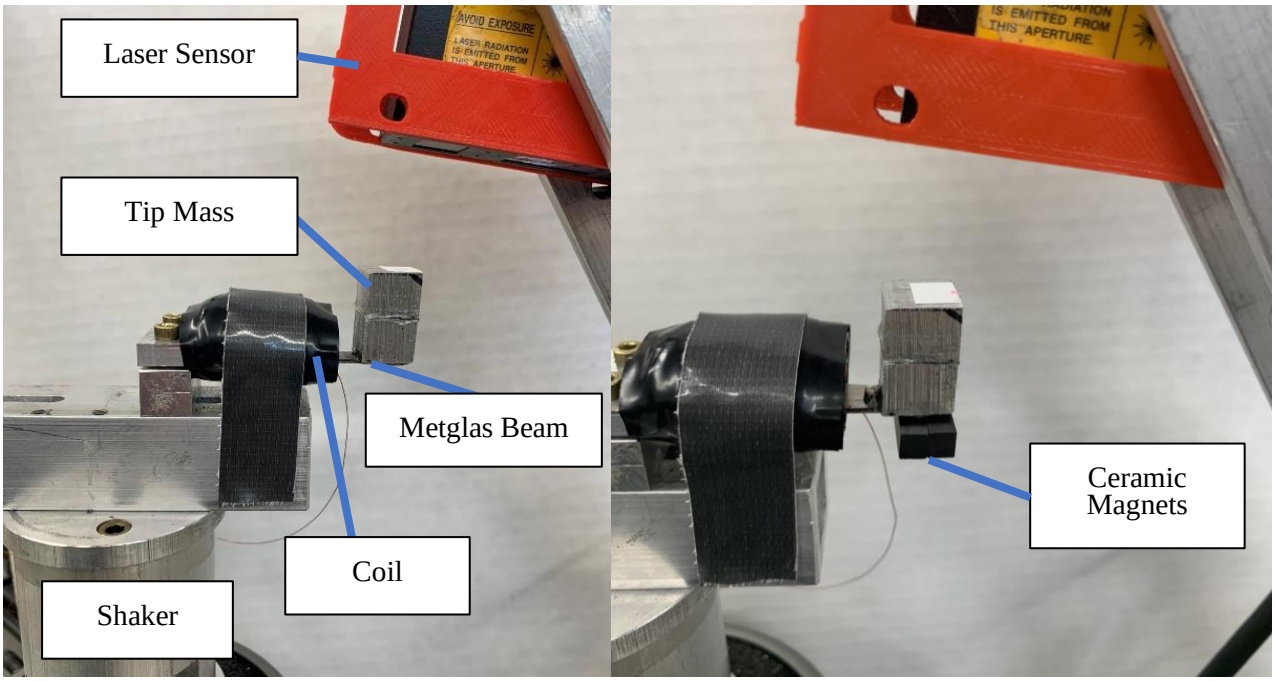

Figure 19: Metglas beams without and with permanent magnets setup

3.2 Determination of 2826MB Beam First Natural Frequencies Using Coil Voltage

As a four-layer Metglas 2826MB laminated stainless steel beam with an 11.28 g tip mass was vibrated through a range of frequencies from 1 Hz to 800 Hz, the pickup coil surrounding the beam's voltage output varied as illustrated in Figure 20. However, at certain excitation frequencies, the voltage spiked. With such a voltage spike it can be assumed that at these points, the beam was deforming at a higher amplitude, as higher deformation in a magnetostrictive materials leads to larger magnetic field changes, which lead to larger induced voltages in a coil. With multiple trials

conducted, the average first natural frequency was found to be about 53.6142 Hz in Table 7. This is about 54% different to the expected theoretical natural frequency of 31.238 Hz, but aligns with the 47.5000 Hz frequency previously measured from the displacement sensor spectrum for the beam.

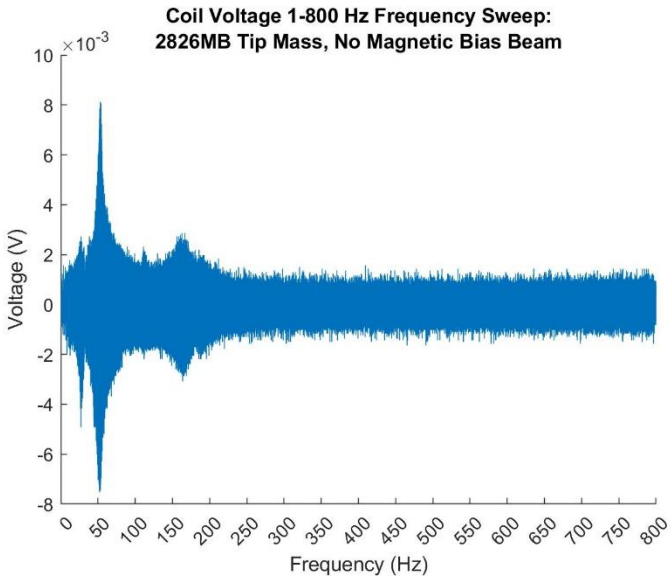

Figure 20: 2826MB beam voltage induced in pickup coil with no magnetic bias

Table 7: First natural frequencies of Metglas 2826MB beam without magnetic bias

Trial	**Frequency of Beam at Maximum Coil Voltage (Hz)**
1	53.1578
2	53.6457
3	54.0391
Average	53.6142

Following these trials, a magnetic bias was introduced to the system through the addition of permanent magnets to the beam tip. The magnets were to align the magnetic domains of the material in order to drive a higher magnetic environmental change. However, these magnets added additional mass to the beam tip, which altered the beam's natural frequency. Since the voltage test followed laser displacement measurements, closely, for the 2826MB without bias, it was assumed that for the bias beam, a frequency sweep would be sufficient to find the first natural frequency. As a result, a voltage sweep test was conducted again from 1-800 Hz. A large voltage peak was observed as shown in Figure 21 with an average of 44.0044 Hz from Table 8. This confers with theory in which the beam's first natural frequency lowers with additional mass on the tip. With the presence of the magnetic bias this peak also becomes sharper.

In Figure 22, the output of the laser displacement sensor was measured over time. Its shape past around 25 Hz is similar to that of the coil's in Figure 21; however, it shows a large displacement in the beginning of the frequency sweep sequence. This large displacement may have been caused by the sudden impulse imparted on the beam by starting the sweep sequence in the shaker. After this initial jump, the displacement seems to decay following the response of a typical damped system imparted with an impulse. Thus, the initial impulse hypothesized from the shaker may hold true as the cause of the initial large displacement. A displacement peak is still shown around 44 Hz in the laser voltage figure, so the displacement and coil voltage confer on a first resonant frequency of 44.0044 Hz for this Metglas 2826MB beam.

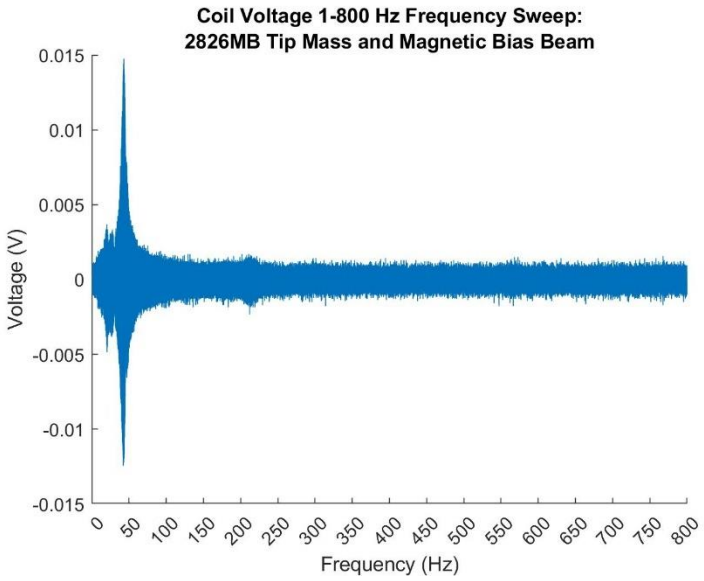

Figure 21: 2826MB beam voltage induced in pickup coil with magnetic bias

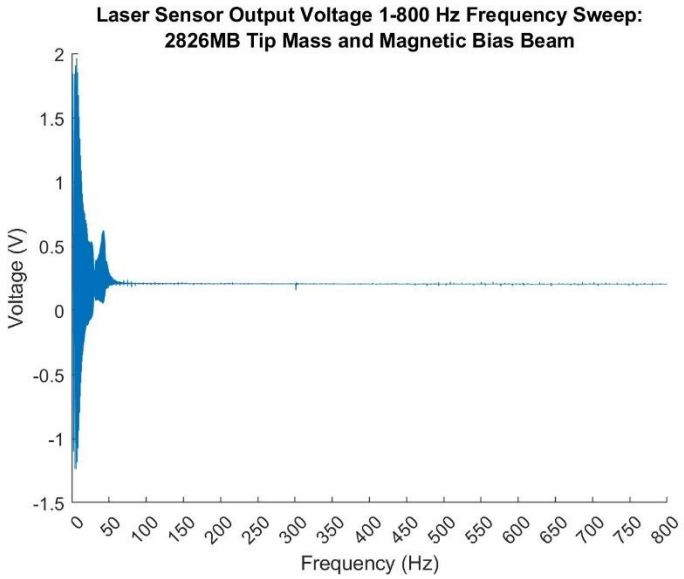

Figure 22: Displacement sensor voltage of vibrating 2826MB beam with magnetic bias in frequency sweep

Table 8: First resonant frequencies of Metglas 2826MB beam with magnetic bias

Trial	Frequency of Beam at Maximum Coil Voltage (Hz)
1	42.9960
2	44.8917
3	44.1255
Average	44.0044

3.3 Determination of 2605SA1 Beam First Natural Frequencies Using Coil Voltage

In a similar manner to the methods discussed in section 3.2, a four-layer Metglas 2605SA1 epoxy laminated beam on stainless steel substrate was observed. With a tip mass of 10.96 g, the beam's first natural frequency was discerned around an average frequency of 58.2743 Hz in Table 9. This value was close to the 51 Hz value determined for the beam from the laser displacement. As expected from this beam's slightly varying beam dimensions and tip mass in comparison to the 2826MB beam, its natural frequency was to be higher than the 2826MB beam. This trend is followed and may have also been caused by the additional thickness of this 2605SA1. This thickness increase was perhaps caused by slightly uneven epoxy distribution in the lamination process. There is a clear peak shown in the coil voltage plot of Figure 23 at the first natural frequency; however, again the laser measured displacement follows a trend of large initial displacement followed by decay. An impulse from initial excitation is again hypothesized as the cause.

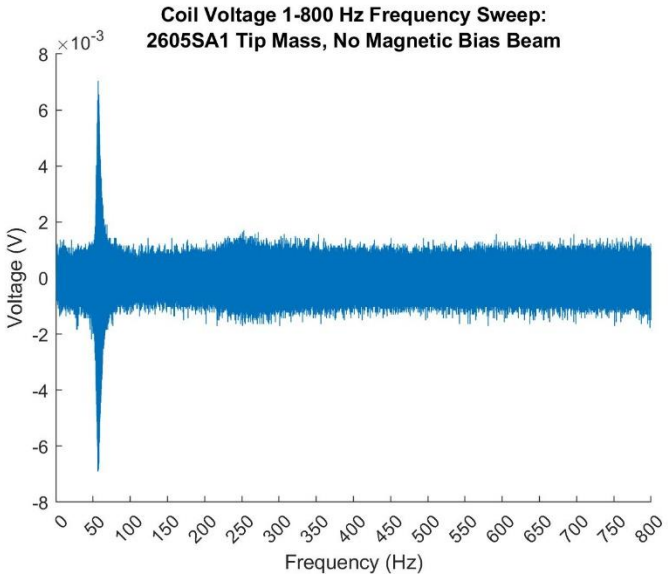

Figure 23: 2605SA1 beam voltage induced in pickup coil with no magnetic bias

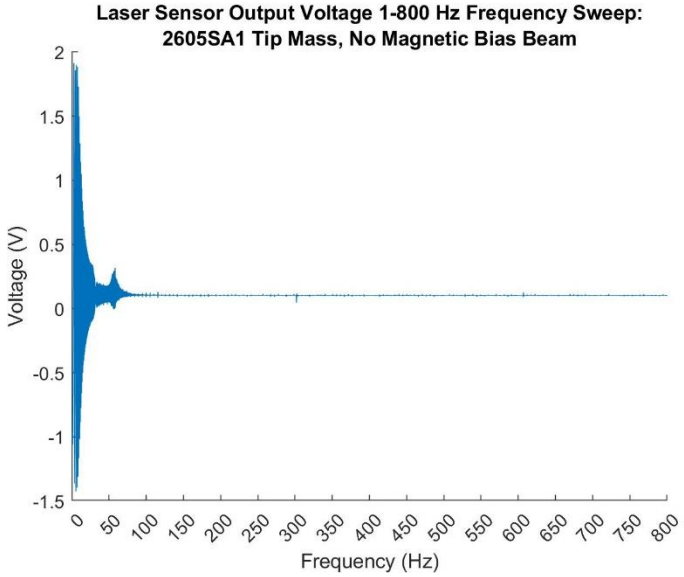

Figure 24: Displacement sensor voltage of vibrating 2605SA1 beam in frequency sweep

Table 9: First resonant frequencies of Metglas 2605SA1 beam without magnetic bias

Trial	Frequency of Beam at Maximum Coil Voltage (Hz)
1	56.9047
2	58.8259
3	59.0922
Average	58.2743

Under the presence of a magnetic bias utilizing the same ceramic magnets as in previous beam trials, the first resonant frequency reduces down to about 49.5586 Hz in Table 10. This reduction not only follows the natural frequency decrease expected with additional tip mass, but also confers with the higher expected natural frequencies of the Metglas 2605SA1 beam due to its dimensions. The voltage spike again becomes sharper with the addition of the magnets in Figure 25. The same decay structure is shown in the measured displacement through the laser sensor in Figure 26.

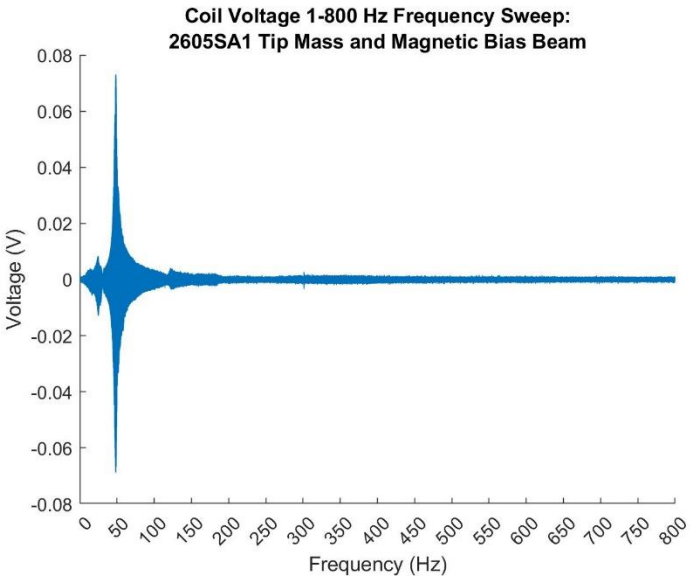

Figure 25: 2605SA1 beam voltage induced in pickup coil with magnetic bias

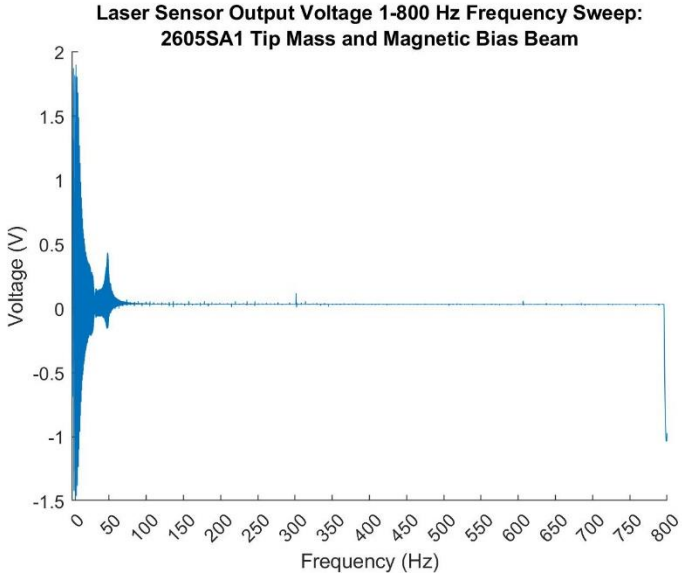

Figure 26: Displacement sensor voltage of vibrating 2605SA1 beam with magnetic bias in frequency sweep

Table 10: First resonant frequencies of Metglas 2605SA1 beam with magnetic bias

Trial	Frequency of Beam at Maximum Coil Voltage (Hz)
1	49.637
2	49.6376
3	49.4013
Average	49.5586

3.4 Bias Magnetic Field Comparison of Energy Harvesting

After determining all of the beam's first natural frequencies using a coil voltage method, the beams were excited at the found resonant frequencies through a continuous sinusoidal movement output by the shaker. Using the same electronic, magnetic, and mechanical system setup as the previous experiments, the maximum voltage harvested from the movement of the Metglas unimorph beam was recorded both with and without the influence of a magnetic bias on both Metglas materials.

For the Metglas 2826MB beam vibrating at 53.6142 Hz, its first resonant frequency, without a magnetic bias, an average of 7.994 mV was harvested. With the addition of the magnetic bias, the Metglas 2826MB beam vibrating at 44.0044 Hz was able to scavenge 13.485 mV. A comparison of the open voltage output across the 220 Ohm resistor is outlined in Table 11. It is assumed that the movement of the tip magnets relative to the coil induced minimal voltage in the coil, thus any voltage it added was neglected in this study. With the introduction of a bias magnetic field in unannealed Metglas 2826MB there was a 68.6820% increase in voltage output with all other beam properties, except tip mass (due to added magnet weight), held the same. Such an increase exemplifies the abilities of even a small magnetic bias such as 0.136 T to improve energy production capabilities of unannealed Metglas 2826MB. Stronger magnets could be employed in

an effort to continue to push the material to its burst region or different magnet setups could be trialed to improve bias effects as has proven to be effective in other magnetostrictive materials like Galfenol [29].

Table 11: Metglas 2826MB maximum voltage generation

Metglas 2826MB	**No Magnetic Bias**	**Magnetic Bias**
1st Res. Freq. (Hz)	53.6142	44.0044
Trial 1 Coil Voltage (mV)	8.131	14.214
Trial 2 Coil Voltage (mV)	7.994	13.257
Trial 3 Coil Voltage (mV)	7.858	12.984
Average (mV)	7.994	13.485

For the Metglas 2605SA1 unimorph beam vibrated at 58.2743 Hz, its first natural frequency, without the influence of a permanent magnet, the average voltage able to be harvested was 7.237 mV. Under the presence of a magnetic bias of 0.136 T on the beam tip, this voltage production increased up to an average of 63.4913 mV under a 49.5586 Hz beam excitation. These voltage outputs again align with the increased abilities of Metglas performance under a bias magnetic field. Metglas 2605SA1's production capabilities increased by 776% with the small bias provided by the magnets. This indicates a large influence of magnetic bias on power production in a Metglas 2605SA1 material system as it does have a higher saturation induction, magnetic saturation values, and magnetic permeability [16]. This material's magnetic property influence

from magnetic bias could be continued to be explored with various magnetic bias strengths and configurations.

Table 12: Metglas 2826MB maximum voltage generation

Metglas 2605SA1	**No Magnetic Bias**	**Magnetic Bias**
1st Res. Freq. (Hz)	58.2743	49.5586
Trial 1 Coil Voltage (mV)	7.452	67.935
Trial 2 Coil Voltage (mV)	7.315	62.809
Trial 3 Coil Voltage (mV)	6.974	59.730
Average (mV)	7.247	63.491

3.5 Metglas Material Comparison of Energy Harvesting

Metglas 2826MB and 2605SA1 are both categorized as magnetostrictive materials indicating they have energy harvesting capabilities through inductance. However, due to their different chemical configurations they lend way to different material properties as outlined in Table 1. This results in different magnetic to electric energy production results. As shown in Table 13, with no magnetic bias present, both materials produced similar voltages in the coil with Metglas 2826MB being slightly larger despite Metglas producers claiming lower magnetostrictive properties [16]. To normalize these beams for differences in their Metglas active areas, their maximum power densities were calculated using equation (11) where V is the open circuit voltage

across the resistor R and Vol_{act} is the volume of the magnetically active materials in this unimorph or Metglas. Using this equation, the power densities also prove to be comparable in size.

There can be seen a large difference in energy production capabilities when a magnetic bias is introduced. The power density of Metglas 2605SA1 increases to 342.4125 $\mu W/cm^3$ which is about 22.8 times larger than the maximum power density produced, 14.990 $\mu W/cm^3$, through Metglas 2826MB. Metglas 2826MB has a lower saturation magnetostriction, which may be why it is less affected by the magnetic bias especially since its permeability unannealed is similar to that of Metglas 2605SA1. Additionally, these materials have differing chemical makeups beyond iron, which may be where these differences can be attributed to as well. By running the same experiments on both materials, it allows for direct comparison of them to occur which can be seen in the plot of Figure 27 where the large increase of 2605SA1 Metglas under magnetic bias is evident.

In previous Metglas energy harvesting experiments, magnetic field annealed Metglas 2605SC was able to produce 900 $\mu W/cm^3$ on a copper unimorph [11]. Also, a steel substrate Metglas 2605SC simulated beam was able to reach a maximum power of 9.4 mW [14]. Even with the magnetic bias 2605SA1 was only able to achieve 342.413 $\mu W/cm^3$ which is below previous Metglas experimentation. This may be because this experiment was run as a way to prove energy harvesting capabilities of unannealed Metglas 2826MB and Metglas 2605A1 in low frequency situations. In addition, these are different Metglas materials than previously tested in a purely cantilever setup. These other experiments also focused on parameter optimization in multiple dimensions while not providing direct Metglas material comparisons. In this study, parameters like the harvesting circuit and thickness ratio were not yet optimized, but instead comparison was the focus. Such optimization could lead to higher power output values as well.

Table 13: Comparison of Metglas 2826MB and 2605SA1

	No Magnetic Bias		Magnetic Bias	
	Metglas 2826MB	**Metglas 2605SA1**	**Metglas 2826MB**	**Metglas 2605SA1**
Average Voltage Harvested (mV)	7.994	7.247	13.485	63.491
Maximum Voltage Harvested (mV)	8.131	7.452	14.214	67.935
Max Power Density (μW/cm3)	4.905	4.120	14.990	342.413
Max Power (mW)	0.301	0.252	0.918	20.978

$$PD = \frac{V^2/R}{Vol_{act}} \tag{11}$$

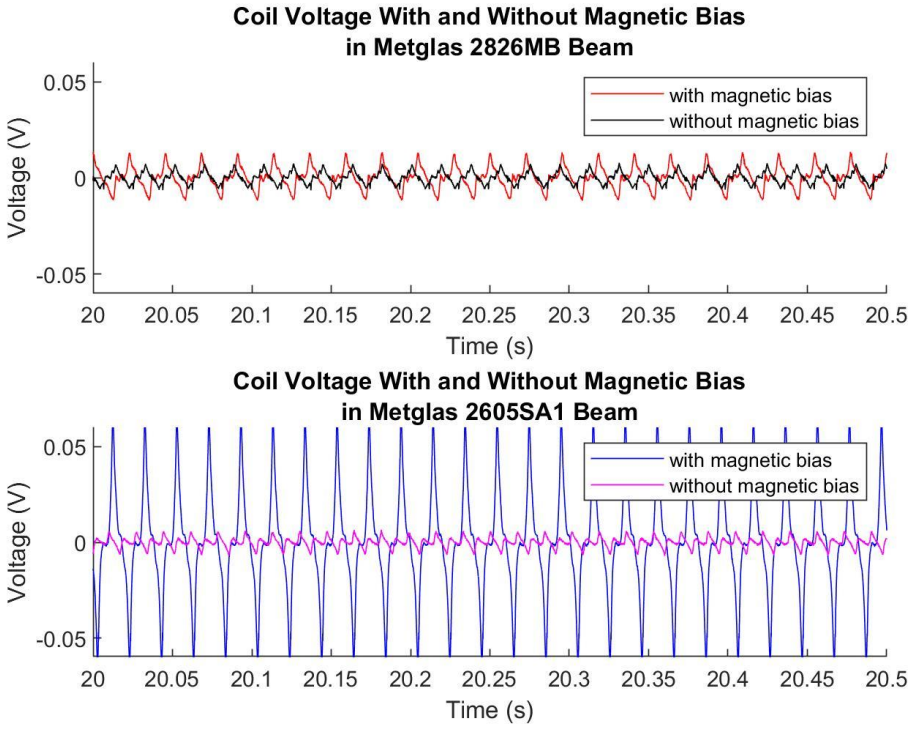

Figure 27: Coil voltage output of Metglas beams with and without magnetic bias

Chapter 4: Concluding Remarks

4.1 Summary and Conclusions

In this research, Metglas 2826MB and 2605SA1 were evaluated for their energy harvesting capabilities as magnetostrictive materials to harness energy from the wind in order to power a wind sensor system. A single layered Metglas 2826MB stainless steel unimorph, four layered Metglas 2826MB stainless steel unimorph, and a four layered Metglas 2605SA1 beam were all vibrationally characterized using a displacement sensor to begin energy harvesting capability exploration. Using frequency spectrum methods, the true resonant frequency of the beam was found to vary from the fundamental theoretical beam bending calculations. The beams were not perfectly clamped and had extra stiffness imparted by the Metglas layers that was not accounted for and may have been the cause of some of the variation between values. In addition, the theoretical equations used may have simplified the problem too much; thus, a more complex problem could be developed in the future or more in-depth simulation modelling to better predict Metglas/stainless steel unimorph beams for a variety of dimensions.

To characterize the energy harvesting capabilities of both Metglas 2826MB and 2605SA1, their natural frequencies were found using a frequency sweep and finding a point of maximum coil output. Such a method proved to converge with the natural frequencies found using the displacement and frequency spectrum method. Beams with and without magnetic biases were then vibrated at their first natural frequencies as a way to find maximum voltage output of the material. With a small magnetic bias present, Metglas 2826MB had an 68.6820% increase in voltage output, while Metglas 2605SA1 had a large increase of 776%, despite both Metglas materials outputting similar voltages without a magnetic bias.

Both materials also had maximum power density values with the presence of a bias magnetic field. Metglas 2826MB had a maximum power density of 14.990 $\mu W/cm^3$ while Metglas 2605SA1 had a maximum power density of 342.413 $\mu W/cm^3$. In comparison, it may be assumed that Metglas 2605SA1 has more promising capabilities for energy harvesting uses; especially for a wind harvesting system. However, it is still performing below the abilities of other forms of Metglas studied in other literature, so further tuning of the circuitry and parameters would need to occur.

Overall, this research has proven the vibrational energy harvesting capabilities of both Metglas 2826MB and 2605SA1 both with and without the presence of a bias magnetic field. Such low power energy harvesting capabilities may not only be useful for the self-powered wind sensor system goal of this project, but could also prove applicable in other vibrational situations, low power sensor systems, or wireless power transmission through induction.

4.2 Future Work

Future work on this project could include determining and modelling more complex Metglas beam resonant frequency systems and equations. Such a system could then be used to make power output predictions. Additionally, further parameters could be explored between the two Metglas materials. Things such as the thickness ratio and bias magnetic field placement may affect the materials in different amounts, as the presence of a bias magnetic field did in this experiment. So, in the interest of creating the most optimal harvester, it would be advantageous to explore all possible combinations of parameters. Similar cantilever beam and coil setups could be attempted in a wind setting so as to see the effects of the materials in less controlled vibrational settings. Additionally, more complex harvesting circuits could be investigated for such a low frequency Metglas system to find an optimal electrical setup to smooth voltage output to transfer

it to a sensor system. Integration of the energy harvesting system to other sensors will allow for a wide variety of applications for this energy harvesting material.

Bibliography

[1] Jarvinen P. Detection of pitot-static icing at high altitudes. 51st AIAA Aerosp. Sci. Meet. New Horiz. Forum Aerosp. Expo., American Institute of Aeronautics and Astronautics; n.d. https://doi.org/10.2514/6.2013-655.

[2] Hubbard JD, Brescoll GP. Aerodynamic investigation of a cup anemometer. UNT Digit Libr 1934. https://digital.library.unt.edu/ark:/67531/metadc172432/m1/4/ (accessed March 21, 2022).

[3] Camp DW, Turner RE, Gilchrist LP. Response tests of cup, vane, and propeller wind sensors. J Geophys Res 1896-1977 1970;75:5265–70. https://doi.org/10.1029/JC075i027p05265.

[4] Grare L, Lenain L, Melville WK. The influence of wind direction on Campbell scientific CSAT3 and Gill R3-50 sonic anemometer measurements. J Atmospheric Ocean Technol 2016. https://journals.ametsoc.org/view/journals/atot/33/11/jtech-d-16-0055_1.xml?tab_body=pdf (accessed March 21, 2022).

[5] Safaei M, Sodano HA, Anton SR. A review of energy harvesting using piezoelectric materials: state-of-the-art a decade later (2008–2018). Smart Mater Struct 2019;28:113001. https://doi.org/10.1088/1361-665X/ab36e4.

[6] Tang X, Wang X, Cattley R, Gu F, Ball AD. Energy harvesting technologies for achieving self-powered wireless sensor networks in machine condition monitoring: a review. Sensors 2018;18:4113. https://doi.org/10.3390/s18124113.

[7] Kök M, Qader İN, Dağdelen F, Aydoğdu Y. A review of smart materials: researches and applications. El-Cezeri Fen Ve Mühendis Derg 2019. https://doi.org/10.31202/ecjse.562177.

[8] Gibbs MRJ. Magnetostriction: 150 years from the discovery. Phys Scr 1992;T45:115–9. https://doi.org/10.1088/0031-8949/1992/T45/024.

[9] Gao C, Zeng Z, Peng S, Shuai C. Magnetostrictive alloys: promising materials for biomedical applications. Bioact Mater 2022;8:177–95. https://doi.org/10.1016/j.bioactmat.2021.06.025.

[10] Deng Z, Dapino MJ. Review of magnetostrictive vibration energy harvesters. Smart Mater Struct 2017;26:103001. https://doi.org/10.1088/1361-665X/aa8347.

[11] Wang L, Yuan FG. Vibration energy harvesting by magnetostrictive material. Smart Mater Struct 2008;17:045009. https://doi.org/10.1088/0964-1726/17/4/045009.

[12] Deng Z, Dapino MJ. Modeling and design of Galfenol unimorph energy harvesters. Smart Mater Struct 2015;24:125019. https://doi.org/10.1088/0964-1726/24/12/125019.

[13] Beeby SP, Tudor MJ, White NM. Energy harvesting vibration sources for microsystems applications. Meas Sci Technol 2006;17:R175–95. https://doi.org/10.1088/0957-0233/17/12/R01.

[14] Mohammadi S, Esfandiari A. Magnetostrictive vibration energy harvesting using strain energy method. Energy 2015;81:519–25. https://doi.org/10.1016/j.energy.2014.12.065.

[15] Learn about Metglas® from our frequently asked questions. Metglas Inc n.d. https://metglas.com/frequently-asked-questions/ (accessed March 31, 2022).

[16] Learn about magnetic materials from Metglas®, Inc. Metglas Inc n.d. https://metglas.com/magnetic-materials/ (accessed April 4, 2022).

[17] Kellogg R, Flatau A. Experimental investigation of Terfenol-D's elastic modulus. J Intell Mater Syst Struct 2008;19:583–95. https://doi.org/10.1177/1045389X07077854.
[18] Clemente C, Davino D. Modeling and characterization of a kinetic energy harvesting device based on Galfenol. Materials 2019;12:3199. https://doi.org/10.3390/ma12193199.
[19] Blevins RD. Formulas for dynamics, acoustics and vibration. John Wiley & Sons, Ltd; 2016.
[20] Stampfli R, Newacheck S, Youssef G. Fully-coupled computational modeling of the dynamic response of 1-3 multiferroic composite structures. Int J Mech Sci 2021;191:106086. https://doi.org/10.1016/j.ijmecsci.2020.106086.
[21] What is strength of carbon steel - definition. Mater Prop 2020. https://material-properties.org/what-is-strength-of-carbon-steel-definition/ (accessed April 9, 2022).
[22] Terfenol-D - ETREMA Products, Inc. TdVib LLC n.d. http://tdvib.com/terfenol-d/ (accessed April 9, 2022).
[23] 10.2: Permeability of some common materials. Eng Libr 2019. https://eng.libretexts.org/Bookshelves/Electrical_Engineering/Electro-Optics/Book%3A_Electromagnetics_I_(Ellingson)/10%3A_Appendices/10.02%3A_Permeability_of_Some_Common_Materials (accessed April 9, 2022).
[24] Ren L, Yu K, Tan Y. Applications and advances of magnetoelastic sensors in biomedical engineering: a review. Materials 2019;12:1135. https://doi.org/10.3390/ma12071135.
[25] Linear coefficient of expansion - an overview | ScienceDirect Topics n.d. https://www.sciencedirect.com/topics/engineering/linear-coefficient-of-expansion (accessed April 13, 2022).
[26] Nondestructive evaluation physics : magnetism n.d. https://www.nde-ed.org/Physics/Magnetism/Demagnetization.xhtml (accessed April 13, 2022).
[27] Jafari H, Ghodsi A, Azizi S, Ghazavi MR. Energy harvesting based on magnetostriction, for low frequency excitations. Energy 2017;124:1–8. https://doi.org/10.1016/j.energy.2017.02.014.
[28] Tan Y, Zhang Y, Ren L. Energy Harvesting from an artificial bone. IEEE Access 2019;7:120065–75. https://doi.org/10.1109/ACCESS.2019.2937120.
[29] Deng Z, Dapino MJ. Modeling and design of Galfenol unimorph energy harvester. Act. Passive Smart Struct. Integr. Syst. 2014, vol. 9057, SPIE; 2014, p. 735–49. https://doi.org/10.1117/12.2047113.